Effect of Strain Hardening on Unloading of a Deformable Sphere Loaded against a Rigid Flat – A Finite Element Study

Biplab Chatterjee, Prasanta Sahoo [1]

Department of Mechanical Engineering, Jadavpur University
Kolkata 700032, India

***Abstract*—The present study considers an elastic-plastic contact analysis during loading-unloading of a deformable sphere with a rigid flat using finite element method. The effect of strain hardening on the contact behavior of a non-adhesive frictionless elastic-plastic contact is analyzed using commercial finite element software ANSYS. To study the strain hardening effect different values of tangent modulus are considered by varying the hardening parameter. The range of hardening parameter is chosen in such a way that most of the practical materials belong in this range. The effect of strain hardening is explained through the results of simulations and compared with elastic perfectly plastic models as well as available loading-unloading models. Analysis has been carried out for deformations up to 200 times the critical interference. It is found that the contact parameters during loading-unloading are not of uniform nature within the range of hardening parameters used in this study. Increased strain hardening results in less residual strain and offer less resistance to full recovery of the original spherical shape. Multiple loading-unloading is also done for two extreme cases of hardening parameters to study the fluctuation of dimensionless interference during subsequent cycles. The contact parameters are found identical with first cycle of loading-unloading.**

I. INTRODUCTION

Strain hardening is an increase in the strength and hardness of the metal due to a mechanical deformation in the metal's microstructure. This is caused by the cold working of the metal. This cold working includes shot-peening, rolling, metal forming and various manufacturing processes. During those processes, loading-unloading is necessary. Due to different extent of strain hardening caused by various processes, the interfacial parameters like contact load, contact area, and residual interference after unloading are different for tribological pairs. Finite element method (FEM) simulations are now used to achieve a deeper understanding of these contact parameters. However, application of FEM technique to quantify the effect of material properties on these contact parameters during loading-unloading is very limited.

Kogut and Etsion [1] (KE Model) first provided an accurate result of elasto-plastic contact of a hemisphere and a rigid flat during loading using finite element method. Jackson and Green [2] (JG Model) extended the KE model to account for the geometry and used five different yield strengths (Y) for their study. Quicksall et al. [3] used finite element technique to model the elastic-plastic deformation of a hemisphere in contact with a rigid flat for various materials such as aluminum, bronze, copper, titanium and malleable cast iron. Brizmer et al. [4] have done elastic-plastic contact analysis between a sphere and rigid flat under perfect slip and full stick conditions for a wide range of material properties using FEM. Sahoo and Chatterjee [5] analyzed the elastic-plastic loading behavior of a sphere against a rigid flat under varying modulus of elasticity. They observed that the materials with Young's modulus to yield strength ratio (E/Y) less than 300 have more variation in contact load as well as in contact pressure than that of the materials with E/Y ratio more than 300 for the same non-dimensionless interference ratio within the elastic-plastic range. Shankar and Mayuram [6] studied the elastic-plastic transition behavior in a hemisphere in contact with a rigid flat accounting for the effect of realistic material behavior in terms of the varying yield strengths and the isotropic strain hardening behavior. However, a detailed study of the effect of strain hardening was not done. Sahoo et al. [7] studied the effect of strain hardening for elastic-plastic contact and inferred that with the increase in strain hardening the resistance to deformation of a material is increased and the material becomes capable of carrying higher amount of load in a smaller contact area.

For unloading, Johnson [8] offered one of the first simple analytical models of unloading of an elastic-plastic spherical indentation contact. Mesarovic and Johnson [9] examined the process of unloading of two elastic-plastic spheres following very large indentation. They assumed that during unloading the deformation is predominantly elastic. So the loading process was solved numerically while the unloading solution was considered analytically. Ye and Komvopoulos [10]

modeled the inverse case of a loading-unloading of a rigid sphere against a elastic-plastic layered media. Li et al. [11] presented a theoretical load-unload model. Etsion et al. [12] performed unloading of an elastic-plastic loaded spherical contact. They provided a model of universal nature, which was independent of the physical and geometrical properties of the sphere. But they did not consider the effect of high yield strength that renders low E/Y ratio and strain hardening. Jackson et al. [13] studied the residual stress and deformation in elastoplastic hemispherical contact with a rigid flat. They also analyzed the effect of material properties on the surface displacement for aluminum and steel spheres. They inferred that the deformation of the aluminum and steel hemispheres followed the same trend; however the values of the normalized displacements were quantitatively quite different. Kadin et al. [14] presented a multiple loading - unloading of an elastic-plastic spherical contact to cover a wide range of loading conditions far beyond the elastic limit. Kadin et al. [15] presented unloading of an elastic-plastic contact of rough surfaces. Ovcharenko et al. [16] performed experimental investigation to calculate the real contact area between a sphere and a flat during loading-unloading and cyclic loading-unloading in the elastic-plastic regime. Du et al. [17] studied the effect of adhesion and plasticity during loading-unloading of a deformable sphere with a rigid flat. Malayalamurthi and Marappan [18] studied the effect of material properties on the residual strains in a sphere after unloading from the elastic-plastic state. It is found that the effects of common material properties on contact parameters are available in the literature. On the other hand, the effect of material properties like strain hardening during loading-unloading is still missing in the literature. The present work is therefore an attempt to quantify the effect of strain hardening on residual interference and load-area behavior during unloading.

II. FINITE ELEMENT FORMULATION

The contact of a deformable hemisphere and a rigid flat is shown in Fig. 1 where the dashed and solid lines represent the situation before and after contact respectively of the sphere of radius R. The figure also shows the interference (ω) and contact radius (a) corresponding to a contact load (P). The contact of deformable sphere with a rigid flat is modeled using finite element software ANSYS 11.0. Due to the advantage of simulation of axi-symmetric problems the model is reduced to a quarter circle with a straight line at its top.

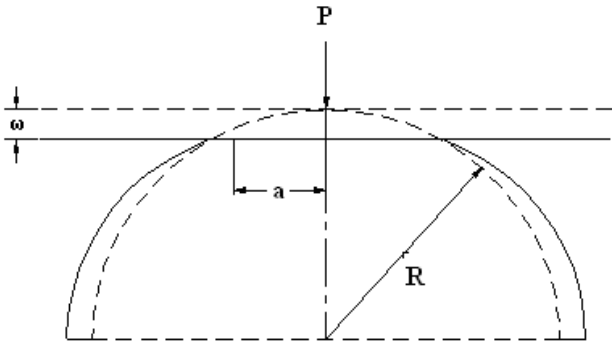

Fig.1. A deformable sphere pressed by a rigid flat

The quarter circle is divided into two different zone, e.g., zone I and zone II. Here zone I is within 0.1R distance from the sphere tip and zone II is the remaining region of the circle outside zone I. these two zones are significant according to their mesh density. The mesh density of zone I is high enough for the accurate calculation of the contact area of the sphere under deformation. Zone II has a coarser mesh as this zone is far away from the contact zone. The meshed model is shown in Fig. 2. The resulting mesh consists of 12986 no of PLANE82 and 112 no of CONTA172 elements. Here the arc of the circle represents the deformable contact surface and the straight line is the rigid flat.

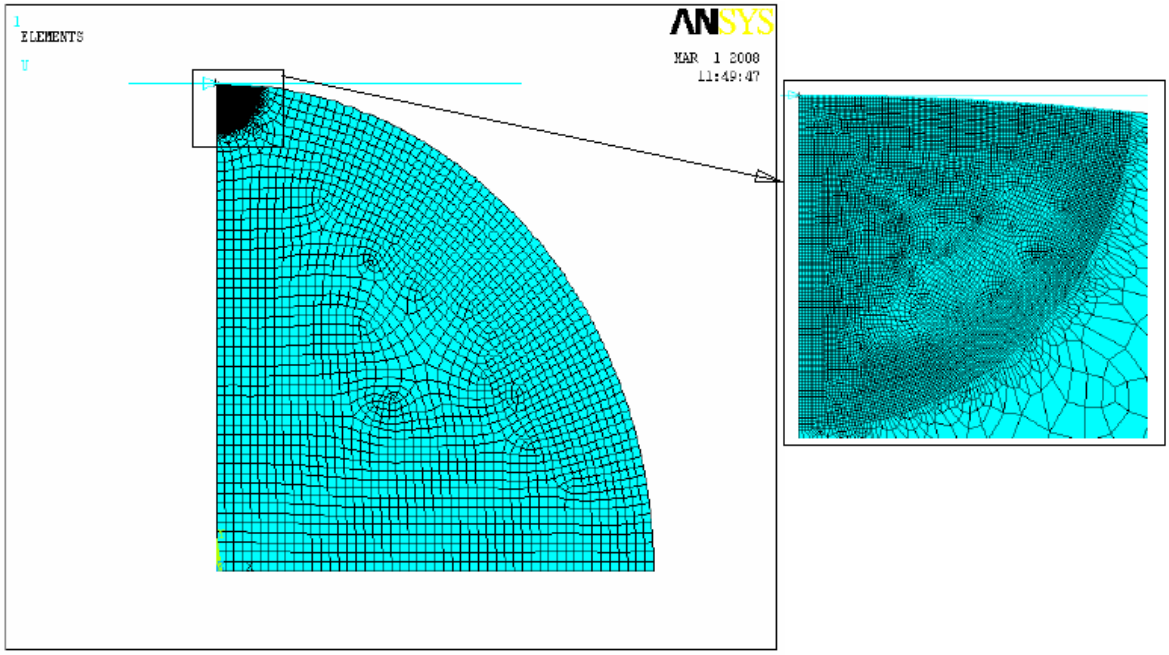

Fig.2. Meshed model of the hemispherical contact

The nodes lying on the axis of symmetry of the hemisphere are restricted to move in the radial direction. Also the nodes in the bottom of the hemisphere are restricted in the in the axial direction due to symmetry. The sphere size is used for this analysis is R = 0.01 m. The material properties used here are Young's Modulus (E) = 70 GPa, Poission's Ratio (ν) = 0.3 and Yeild stress (σ_y) = 100 MPa. Here a frictionless rigid-deformable contact analysis is performed. In this analysis a bilinear material property, as shown in Fig. 3, is provided for the deformable hemisphere. To study the strain hardening effect we have taken different values of tangent modulus (E_t). The Tangent Modulus (E_t) is varied according to a parameter which is known as Hardening parameter and defined as, $H = \frac{E_t}{E - E_t}$. The value of H is taken in the range $0 \le H \le 0.5$ as most of the practical materials falls in this range. The value of H equals to zero indicates elastic perfectly plastic material (E_t) behavior which is an idealized material behavior. The hardening parameters used for this analysis and their corresponding values are shown in Table 1.

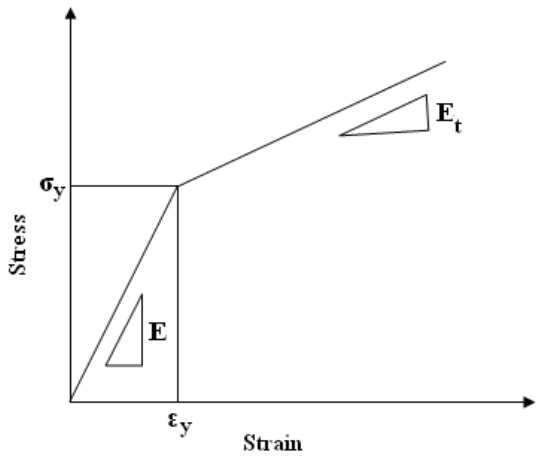

Fig.3. Stress-strain diagram for a material having bilinear isotropic properties

TABLE 1

DIFFERENT H AND E_t VALUES USED FOR THE STUDY OF STRAIN HARDENING EFFECT

H	E_t in %E	E_t (GPa)
0	0.0	0.0
0.1	9.0	6.3
0.2	16.7	11.7
0.3	23.0	16.1
0.4	28.6	20.0
0.5	33.0	23.1

The wide range of values of tangent modulus is taken to make a fair idea of the effect of strain hardening effect in single asperity contact analysis. The solution type is chosen as large deformation static analysis. Here we have applied displacement on the target surface and the force on the hemisphere is found from the reaction solution. As this is an axi-symmetric analysis the force is calculated on a full scale basis. The radius of contact area is found from the last activated node for a particular analysis. In our analysis we have validated our mesh configuration by iteratively increasing the mesh density. The mesh density is increased by 1% until the contact force and contact area is differed by less than 1% between the iterations. In addition to the mesh convergence the model also compared with the Hertz elastic solution. The results of contact load are differed by maximum 3% and contact radius by not more than 5% below the critical interference.

The solution consists of two stages. In the first one we have applied a displacement on the rigid flat by a dimensionless interference $\omega^* = \omega / \omega_c$. During this stage the interference ω is gradually increased up to a desired maximum value, ω_{max}, and the contact load, the real contact area reach their maximum value P_{max}, A_{max} respectively. The second stage consists of the unloading process, where the interference, ω, is gradually reduced. When the unloading process is completed, the contact load, real contact areas fall to zero. However, the original un-deformed spherical geometry is not fully recovered. The deformed shape may be characterized by a residual interference (ω_{res}) as shown in Fig. 4.

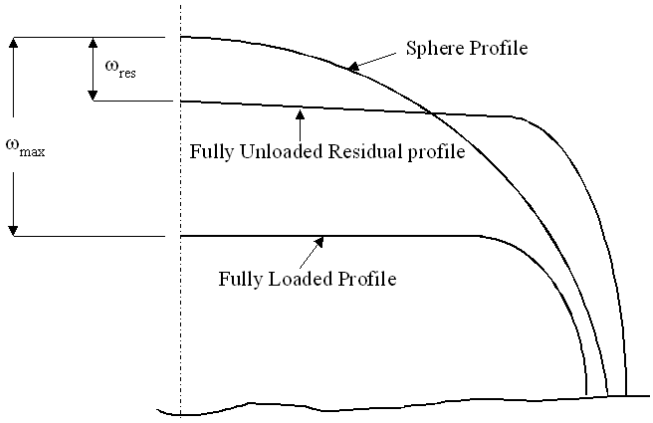

Fig.4 Three different profiles of the sphere

III. RESULTS AND DISCUSSION

As discussed earlier the strain hardening effect is studied by varying the hardening parameter which in turn changes the value of tangent modulus while other material properties are kept constant. The model is validated by comparing the results for elastic perfectly plastic material condition, i.e. for $H = 0$, with the results of KE model [1]. The results are normalized according to the following normalization scheme. Interference (ω) is normalized by the critical interference (ω_c), provided by Chang et al. [19]. The critical interference is defined as,

$$\omega_c = \left(\frac{\pi K S}{2E^*}\right)^2 R$$

Where, K is the hardness coefficient [$K = 0.454 + 0.41\nu$], S is the hardness of the material, according to Tabor [20] S is related to yield strength by $S = 2.8\sigma_y$ and E^* is the equivalent young's Modulus, $E^* = E/(1-\nu^2)$ in this case [E is the young modulus and ν is the Poisson's ratio of the deformable body]. The contact load (P) is normalized by the critical contact load (P_c), i.e., load corresponding to critical interference and P_c is written as,

$$P_c = \frac{4}{3} E^* R^{1/2} \omega_c^{3/2}$$

The contact area (A) is normalized by the critical contact area (A_c), i.e., area corresponding to critical interference and A_c is written as,

$$A_c = \pi R \omega_c$$

The dimensionless parameters are as follows: $\omega^* = \omega/\omega_c$, $P^* = P/P_c$, $A^* = A/A_c$. The results for elastic perfectly plastic material behavior are compared with the results of Kogut and Etsion [1]. The calculated contact areas are exactly matched in the elastic and certain portion of the elastic plastic region and we found a maximum of 1% difference with the results KE model.

In case of load vs. displacement we found there is a maximum of 3% difference with the results of KE model. It may be noted here that Kogut and Etsion have done this analysis for a large no of sphere radius in the range of $0.1 \le R \le 10$ (mm) as well as for a large no of material properties in the range $100 \le (E/\sigma_y) \le 1000$ and they have also found differences in their results up to 3%.

Fig 5(a) to 5(d) present the dimensionless elastic-plastic load displacement results for the loading-unloading process in terms of P^* vs. ω^*. It shows that with the increase in tangent modulus value the contact load increases at a particular interference value. The numerical results of the unloading

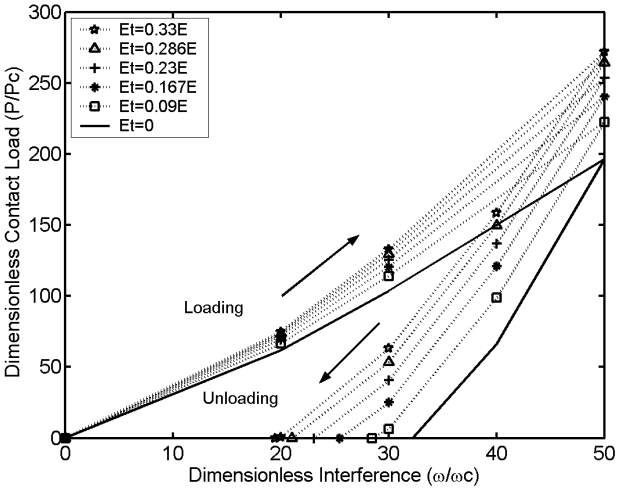

5(a)

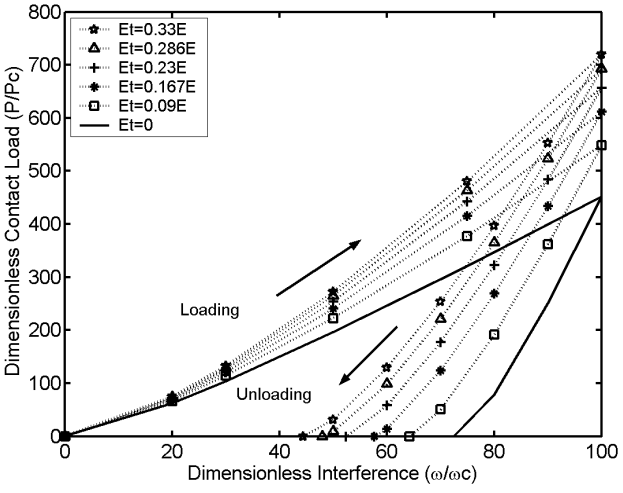

5(b)

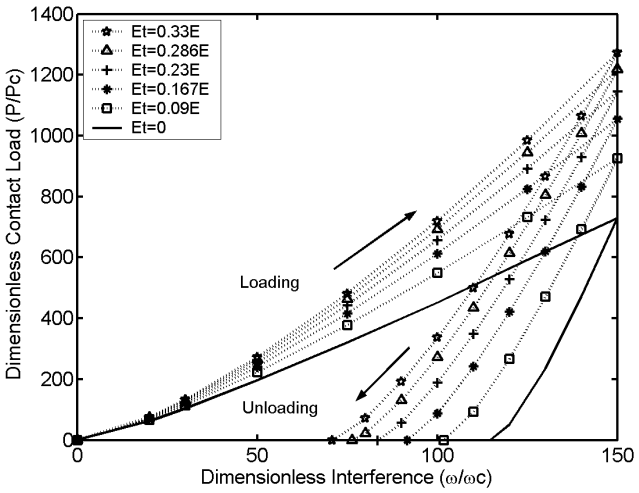

5(c)

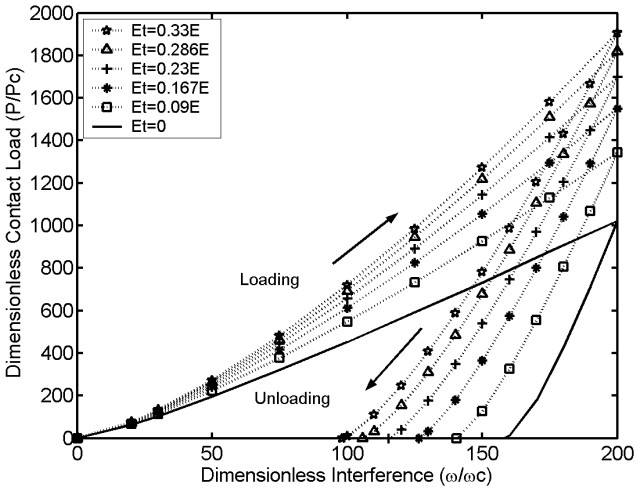

5(d)

Fig.5. Dimensionless contact load –unload from different dimensionless interferences (a) ω_{max}= 50 (b) ω_{max}= 100 (c) ω_{max}= 150 (d) ω_{max} = 200

process initiated from four representative ω_{max}^* (ω_{max}/ω_c) values of 50, 100, 150, 200 respectively are shown. When the unloading process is completed the contact load falls to zero at certain non dimensional interference ω_{res}^* (ω_{res}/ω_c). It is clear from the figures that this ω_{res}^* increases with the decrease of strain hardening (tangent modulus.) irrespective of maximum loading ω_{max}^*; from which unloading started. Though difference of ω_{res}^* with the variation of strain hardening increases with the increase in ω_{max}^*.

Fig. 6(a) to 6(d) represent the dimensionless contact area displacement results for the loading-unloading process in terms of A* vs. ω*. The plot shows a non-linear behavior between the contact area and interference as the results are in the elasto-plastic and fully plastic region. With the increase in tangent

modulus value the contact area decreases at a particular interference value. The numerical results of the unloading process initiated from four representative ω_{max}* values of 50, 100, 150, 200 respectively are shown. The contact area increases just in the vicinity from where unloading starts. This is due to the fact that when plastically deformed hemisphere is unloaded, the elastic material attempts to restore its original shape.

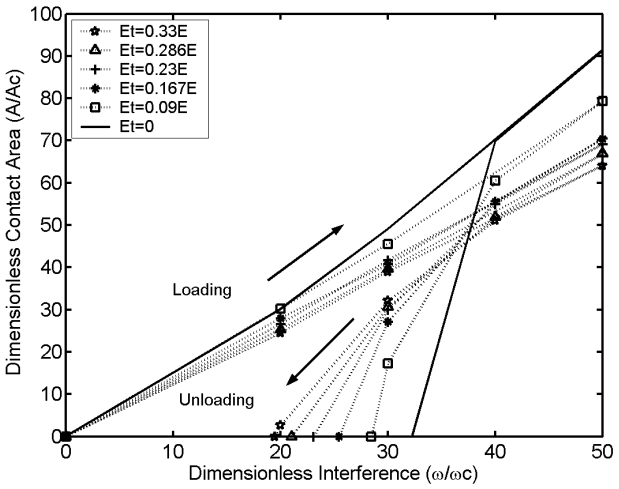

6(a)

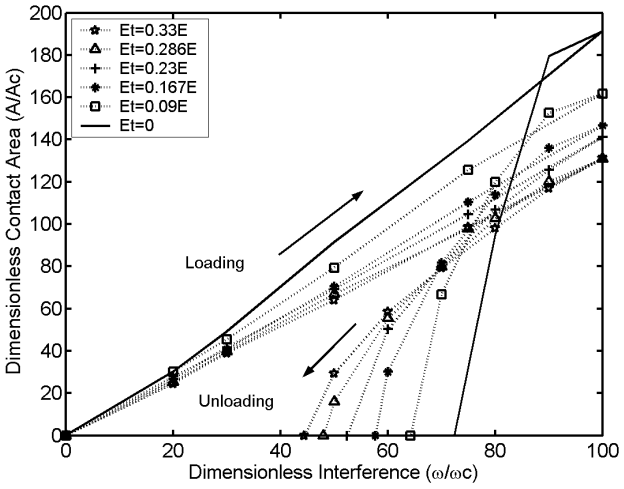

6(b)

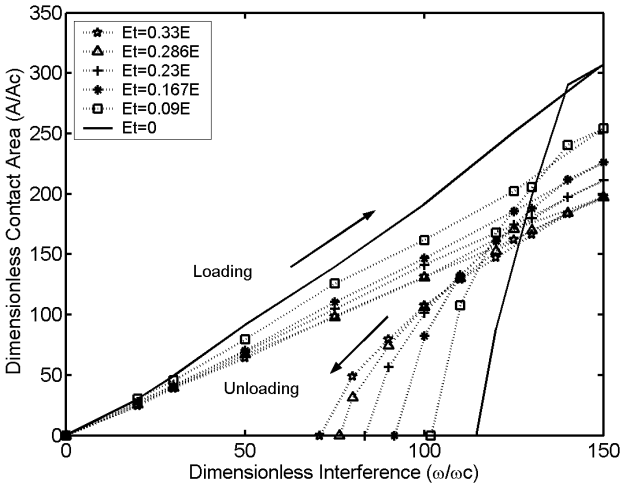

6(c)

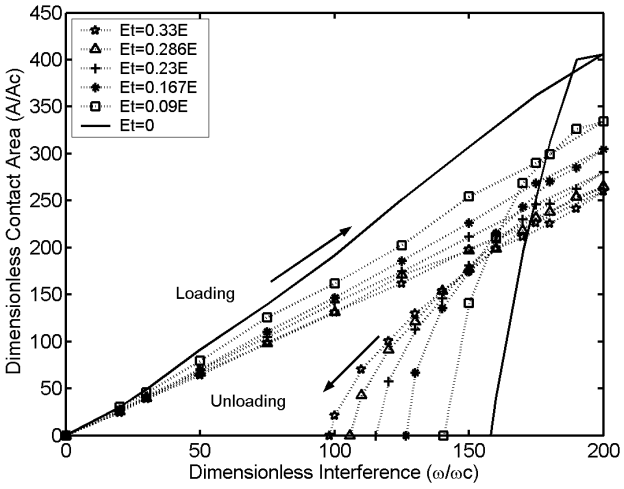

6(d)

Fig.6. Dimensionless contact area vs. interference unloaded from different dimensionless interferences (a)ω_{max}=50 (b) ω_{max}=100 (c) ω_{max}= 150 (d) ω_{max} =200

Fig.7 is the plot of percentage difference in dimensionless residual interference with that of elastic perfectly plastic model. From the fig., the variation of hardening parameters shows that for a small hardening parameter $H = 0.1$ (E_t=0.09E) the dimensionless residual interference (ω^*_{res}) is about 11% lower than that of elastic perfectly plastic material. While for the large hardening parameter $H = 0.5$ (E_t=0.33E), the ω^*_{res} is about 39% lower. It is clear from the fig that when tangent modulus is 2% of E, as used by Etsion et al. [12] the percentage variation of ω^*_{res} is negligible and the results are quite close to that of elastic perfectly plastic material. Thus the present finite element results indicate that higher hardening offer less resistance to full recovery of the original spherical shape.

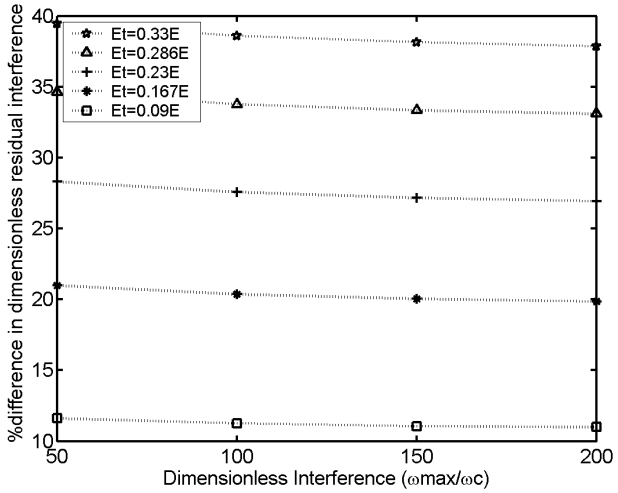

Fig.7 Percentage difference in dimensionless residual interference (ω^*_{res}) with elastic perfectly plastic model

Fig. 8(a) to 8(d) present the dimensionless contact area, A^* vs. dimensionless contact load, P^* during loading and unloading. The numerical results of the unloading process initiated from four representative ω_{max}* values of 50, 100, 150, 200 respectively are shown. Here it is observed that the contact area decrease at a particular load for a material having higher tangent modulus value than that of a material having lower one. During unloading, it is clear from the plots that for a given contact load, the real contact area is larger than the contact area during loading. The differences in real contact area between loading and unloading are larger for higher maximum loading interference, ω^*_{max}. The average contact pressure during unloading is smaller than that of during loading. To support a given contact load with smaller average contact pressure it requires larger real contact area as indicated in Fig. 8(a) to 8(d).

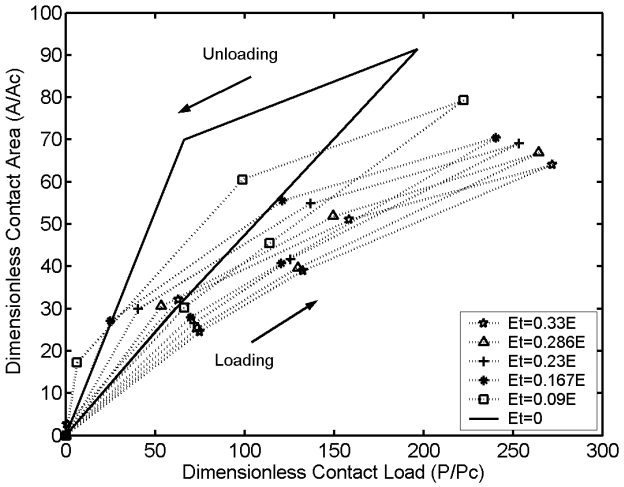

8(a)

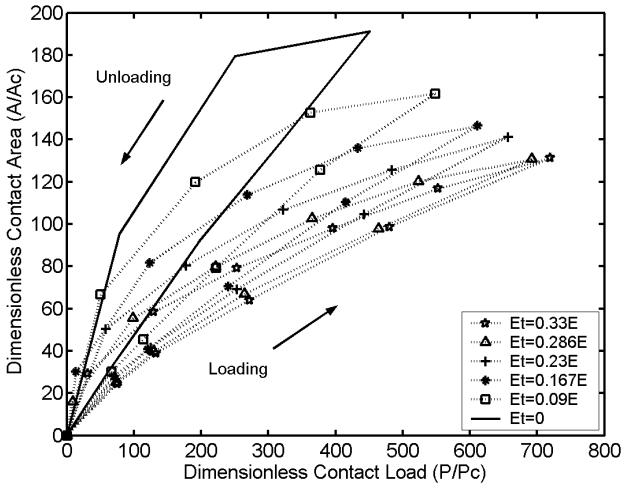

8(b)

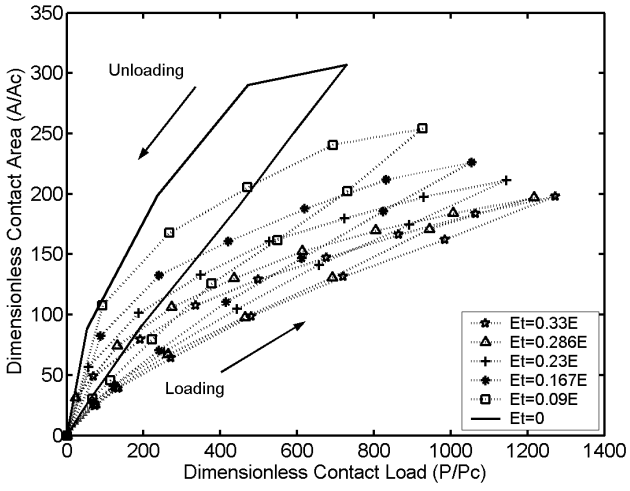

8(c)

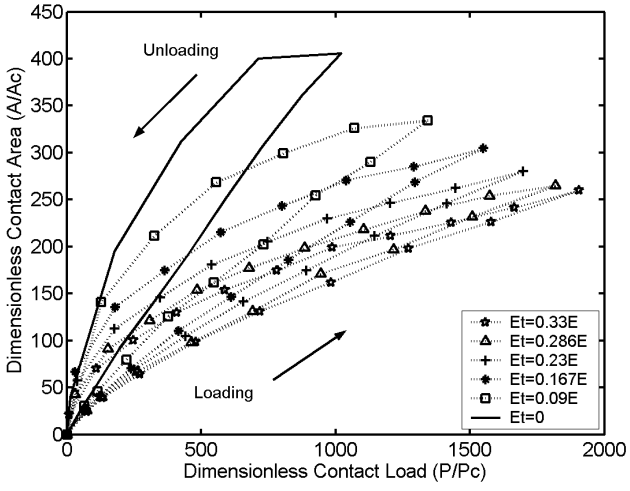

8(d)

Fig.8 Dimensionless contact area vs. dimensionless contact load, unloaded from different dimensionless interference (a)ω_{max}=50 (b) ω_{max}=100 (c) ω_{max}= 150 (d) ω_{max} =200

Fig. 9(a) shows the multiple loading unloading plot of P* vs. ω* up to ω^*_{max}=200 (P*=1025), for elastic perfectly plastic material. Here the dimensionless contact load obtained after the second loading is same that of after first loading. The first unloading and second loading path is also same. Kadin et al. [14] observed different first unloading and second loading path when loaded up to P*=450 to study the dimensionless equivalent stress. Fig 9(b) is another multiple loading-unloading plot of P* Vs ω* for the large hardening parameter $H = 0.5$ (Et=0.33E). Here also the observation is identical with that of Fig 9(a).

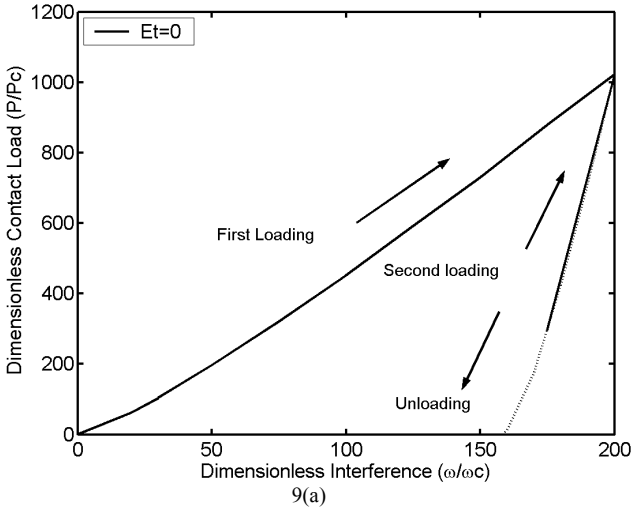

9(a)

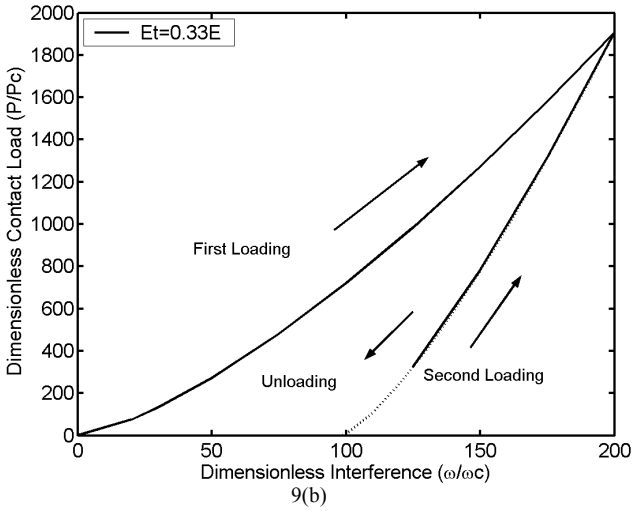

9(b)

Fig.9. Dimensionless contact load vs. dimensionless interference during the process of multiple loading for two different tangent modulus; loaded up to ω^*_{max}=200

Fig. 10 presents the value of ω^*_{res} (ω_{res} / ω_{max}) as a function of ω^*_{max}. Etsion et al. [12] used 2% strain hardening. The plot of "Etsion 2005" in Fig. 10 presents the empirical relation provided by Etsion et al. [12]. Our results correlate well with the findings of Etsion et al. They defined the dimensionless residual interference (ω^*_{res} = $\omega_{res}/\omega_{max}$) as an "elastic-plastic loading (EPL) index". From this graph it can be observed that the EPL index increases with the decrease of tangent modulus (strain hardening). So higher Hardening results in lower residual strain.

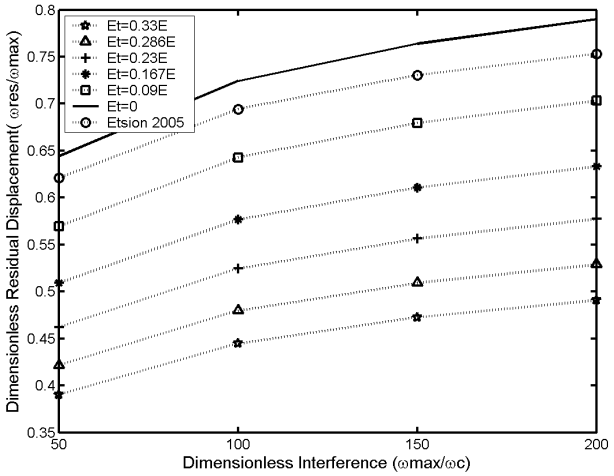

Fig.10. Dimensionless residual interference vs. dimensionless maximum interference

IV. CONCLUSIONS

The loading-unloading of a deformable sphere loaded by a rigid flat is analysed for a wide range of strain hardening. The result for different tangent modulus clearly shows that a generalized solution cannot be applicable for all kind of material. It is observed that higher tangent modulus (strain hardening) results lower residual interference when unloaded from a particular dimensionless interference; which in turn offers less resistance to full recovery of the original shape. The elastic-plastic loading index (EPL index), which may serve as a measure of the level of plasticity of loaded sphere is also increasing with the decrease in hardening parameter. It is also observed that for same real contact area the load carrying capacity also increases with the increase in strain hardening during loading-unloading. The main conclusion of the present work is that the parameter strain hardening should be taken care of appropriately to get the accurate prediction of contact behaviour during loading-unloading.

REFERENCES

[1] L. Kogat, and I. Etsion, "Elastic-plastic contact analysis of a sphere and a rigid flat", *ASME J. Appl. Mech*., vol. 69, pp. 657-662, 2002

[2] R. L. Jackson, and I. Green, "A finite element study of elastic-plastic hemispherical contact against a rigid flat", *ASME J. Tribol*., vol. 46, pp. 383-390, 2003.

[3] J. J. Quicksall, R. L. Jackson, and I. Green, "Elasto-plastic hemispherical contact models for various mechanical

properties", *Proc. Instn. Mech. Engrs., Part J: J. Engg. Tribol*., vol. 218, pp. 313-322, 2004.

[4] V. Brizmer, Y. Kligerman, and I. Etsion, "The effect of contact conditions and material properties on the elasticity terminus of a spherical contact", *Int. J. Solid Struct*., vol. 43, pp. 5736-5749, 2006.

[5] P. Sahoo, and B. Chatterjee, "A finite element study of elastic-plastic hemispherical contact behavior against a rigid flat under varying modulus of elasticity and sphere radius", *Engineering*, vol. 2, pp. 205-211, 2010.

[6] S. Shankar, and M. M. Mayuram, "Effect of strain hardening in elastic-plastic transition behavior in a hemisphere in contact with a rigid flat", *Int. J. Solids Struct*, vol. 45, pp. 3009-3020, 2008.

[7] P. Sahoo, B. Chatterjee, and D. Adhikary, "Finite element based Elastic-plastic contact behavior of a sphere against a rigid flat-effect of strain hardening", *Int. J. Engg. and Tech*., vol. 2(1), pp. 1-6, 2010.

[8] K. L. Johnson, *Contact Mechanics*, Cambridge University Press, Cambridge, MA, 1985.

[9] S. D. Mesarovic, K. L. Johnson, "Adhesive contact of elastic-plastic spheres", *J. Mech. Phys. Solids*., vol. 48(10), pp. 2009-2033, 2000.

[10] N. Ye, K. Komvopoulos, "Effect of residual stress in surface layer on contact deformation of elastic-plastic layered media", *ASME. J. Tribol*, vol. 125(4), pp. 692-699, 2003.

[11] L. Y. Li, C.Y. Wu, and C. Thornton, "A theoretical model for the contact of elastoplastic bodies", *Proc. Instn. Mech. Engrs*., vol. 216 (Part C), pp. 421-431, 2002.

[12] I. Etsion, Y. Kligerman, and Y. Kadin, "Unloading of an elastic-plastic loaded spherical contact", *Int. J. Solid Struct*., vol. 42, pp. 3716-3729, 2005.

[13] R. Jackson, I. Chusoipin, and I. Green, "A finite element study of the residual stress and deformation in hemispherical contacts", *ASME. J. Tribol*, vol. 127, pp. 484-493, 2005.

[14] Y. Kadin, Y. Kligerman, and I. Etsion, "Multiple loading-unloading of an elastic-plastic spherical contact", *Int. J. Solids Struct*., vol.43, pp. 7119-7127, 2007.

[15] Y. Kadin, Y. Kligerman, and I. Etsion, "Unloading an elastic-plastic contact of rough surfaces", *J. Mechanics and Phys. Solids*., vol. 54 , pp. 2652-2674 , 2006 .

[16] A.Ovcharenko, G. Halperin, G. Verberne, and I. Etsion, "In situ investigation of the contact area in elastic-plastic spherical contact during loading-unloading", *Tribol. Letters*, vol. 25(2), pp. 153- 160, 2007.

[17] Y. Du, L. Chen, N. E. McGruer, G. G. Adams, I. Etsion, " A finite element model of loading and unloading of an asperity contact with adhesion and plasticity", *J. colloid and Interface Science*, vol. 312, pp. 522-528, 2007.

[18] R. Malayalamurthi, and R. Marappan, "Finite element study on the residual strains in a sphere after unloading from the elastic-plastic state", *Int. Journal for computational Methods in Engineering Science and Mechanics*, vol. 10(4), pp. 277-281, 2009.

[19] W. R. Chang, I. Etsion, and D. B. Bogy, "An elastic-plastic model for the contact of rough surfaces", *ASME J. Tribol*., vol. 109, pp. 257-263, 1987.

[20] D. Tabor, *The Hardness of Metals*, Clarendon Press, Oxford, 1951.